2

Fusion of PET and MRI for Hybrid Imaging

Zang-Hee Cho, Young-Don Son, Young-Bo Kim, and Seung-Schik Yoo

Summary. Recently, the development of the fusion PET-MRI system has been actively studied to meet the increasing demand for integrated molecular and anatomical imaging. MRI can provide detailed anatomical information on the brain, such as the locations of gray and white matter, blood vessels, axonal tracts with high resolution, while PET can measure molecular and genetic information, such as glucose metabolism, neurotransmitter-neuroreceptor binding and affinity, protein–protein interactions, and gene trafficking among biological tissues. State-of-the-art MRI systems, such as the 7.0 T whole-body MRI, now can visualize super-fine structures including neuronal bundles in the pons, fine blood vessels (such as lenticulostriate arteries) without invasive contrast agents, in vivo hippocampal substructures, and substantia nigra with excellent image contrast. High-resolution PET, known as High-Resolution Research Tomograph (HRRT), is a brain-dedicated system capable of imaging minute changes of chemicals, such as neurotransmitters and –receptors, with high spatial resolution and sensitivity. The synergistic power of the two, i.e., ultra high-resolution anatomical information offered by a 7.0 T MRI system combined with the high-sensitivity molecular information offered by HRRT-PET, will significantly elevate the level of our current understanding of the human brain, one of the most delicate, complex, and mysterious biological organs. This chapter introduces MRI, PET, and PET-MRI fusion system, and its algorithms are discussed in detail.

2.1 Introduction

Among the modern medical imaging technologies, Positron Emission Tomography (PET) and Magnetic Resonance Imaging (MRI) are considered to be the most powerful diagnostic inventions. In the 1940s, modern medical imaging technology began with advancements in nuclear medicine. In the early 1970s, by combining the diagnostic properties of X-rays with computer technology, scientists were able to construct 3D images of the human body in vivo for the first time, prompting the birth of the Computed Tomography (CT). The emergence of CT was an important event that motivated scientists to invent PET and MRI. These imaging tools were not based on simple modifications

T.M. Deserno (ed.), *Biomedical Image Processing*, Biological and Medical Physics, Biomedical Engineering, DOI: 10.1007/978-3-642-15816-2_2,

of existing techniques or devices. Instead, they are the new medical imaging modalities that were the result of the combined effort of numerous scientific disciplines such as physics, mathematics, chemistry, computer science, biology, medicine, and pharmacology.

Initially, PET was based on somewhat primitive form of positron imaging device created in 1953 by Gordon Brownell et al. Massachusetts Institute of Technology (MIT) and then newly born concept of the CT. The first modern PET device was developed by two groups of scientist. One was at University of California at Los Angeles (UCLA) in the mid 1970s by Cho et al [1] and the other was by Ter-Pogossian & Phelps at Washington university, St. Louis [2]. Subsequently, a new detector material, Bismuth-Germanate (BGO) was introduced for use in high-resolution imaging [3]. Today, most commercial PET scanners have adopted the ring-type detector system, based on the use of BGO or Cerium-doped Lutetium Oxyorthosilicate (LSO) scintillators [4]. These PET systems now have spatial resolutions of 5–6 mm at FWHM (Fig. 2.1).

The development of MRI was based on Nuclear Magnetic Resonance (NMR), explored in 1940s by Felix Bloch at Stanford University and Edward Mills Purcell at Harvard University. The first principles of MRI were proposed in 1973 by Paul Lauterbur, and necessary image reconstruction algorithm were developed in the mid 1970s by Richard Ernst. For their achievements, Ernst received 1990 the Nobel Prize in Chemistry, and in 2003, Lauterbur and Mansfield won Nobel Prize in Physiology or Medicine. Much of the MRIs

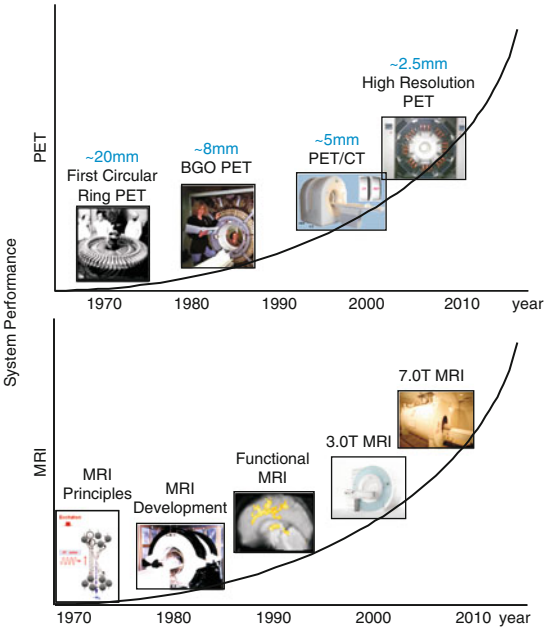

Fig. 2.1. *Historical development of PET and MRI.* The exponential increase of system performance is visualized. The ordinate shows resolution and field strength for PET (*top*) and MRI (*bottom*), respectively

rapid success can be attributed to its non-invasiveness and tissue discrimination capability in the brain. Continuous hardware and software advancements have followed, and new MRI scanners boast sub-millimeter resolution with excellent contrast. The strength of the magnetic field used in the device is described with a unit of Tesla (T) or Gauss G. 1 T is equal to 10,000 G. Although currently available MRI in the market for humans use is up to 8 T, only 4 T is permitted for clinical use by the Food and Drug Administration (FDA) of the United States.

The invention of PET and MRI changed the scene of modern medicine and was perhaps one of the greatest achievements in medicine and the biology. This chapter provides a brief introduction of the basic principles of MRI and PET, followed by an overview of state-of-the-art PET and MRI systems. Subsequently, we described the complementary use of these two devices and technical aspects related to the new PET/MRI fusion system, which has been recently developed, and potential applications are discussed.

2.2 Positron Emission Tomography

2.2.1 Basic Principles

PET is an imaging system that detects two annihilation photons or gamma rays originating from the tracer compounds labeled with positron-emitting radionuclides, which are injected or administered into the subject. Many proton-rich radioisotopes may decay via positron β^+-decay, in which a proton in the nucleus decays to a neutron by emission of a positron and a neutrino. The decay product has one atomic number less than the parent. Examples of radionuclides which undergo decay via positron emission are shown in Table 2.1 [5].

Positron-emitting radionuclides possess an important physical property that makes PET a unique high-resolution molecular imaging device. That is the directionality or collinearity of two simultaneously emitted photons by the annihilation process. When the emitted positron collides with a nearby electron, they annihilate and produce two annihilation photons of 511 keV. The two annihilation photons, which are identical to two gamma photons with 511 keV of energy, then travel in nearly exact opposite directions of

Isotope	Half life (min)	Positron energy maximum (MeV)	Positron range in water (mm)
^{11}C	20.30	0.96	1.1
^{13}N	9.97	1.19	1.4
^{15}O	2.03	1.70	1.5
^{18}F	109.80	0.64	1.0
^{68}Ga	67.80	1.89	1.7
^{82}Rb	1.26	3.15	1.7

Table 2.1. *Radionuclides and their physical properties.* The positron range is given at FWHM

each other. This near collinearity of the two annihilation photons allows to identify the location of the annihilation event or the existence of positron emitters through the detection of two photons by detectors poised exactly on opposite sides of the event, which are contacted by the photons at nearly the same time. This simultaneity also plays an important role for the coincident detection.

A set of detectors converts the high-energy photons into electrical signals that are subsequently processed by signal processing electronics. For detection of these two annihilation 511 keV photons, two scintillation detectors are coupled to an individual Photo-Multiplier Tube (PMT), pulse timer and amplitude analyzer. The detectors of current PET systems are made of inorganic materials called scintillation detectors. Scintillators convert the incident gamma quantum into a large number of light photons. The scintillator must be made of a highly dense material with high atomic number to maximize the gamma photon absorption. In the early development of PET and up to the late 1970s, NaI(Tl) was a commonly used for scintillation detectors. Currently, most modern PET use BGO [3]. While BGO has larger absorption power, LSO has a faster response time and more light output. The light, visible photons, from these scintillators are converted to electrical signals by the PMT or equivalent device. The PMT multiplies the weak signals from the scintillation detectors to electrically detectable signals with both pulse timing and amplitude. Although PMT is the most widely used light photon amplifier, more recently semiconductor type PMTs, such as an Avalanche Photodiode (APD) and the Silicon Photomultiplier (SiPM) have been developed and are in use. A semiconductor type PMT has the advantage over conventional PMTs due to its non-magnetic properties, which supports use in MRI environments, but it has several disadvantages in rigidity and stability (Fig. 2.2).

The amplified electrical signals from PMTs, as electrical pulses, are analyzed to determine when the signal occurred and whether the signal is above a certain threshold. When the valid PET signal is generated by annihilation photons of 511 keV that pass the energy threshold, time information is recorded and used for coincident time analysis. The detected pulses are then

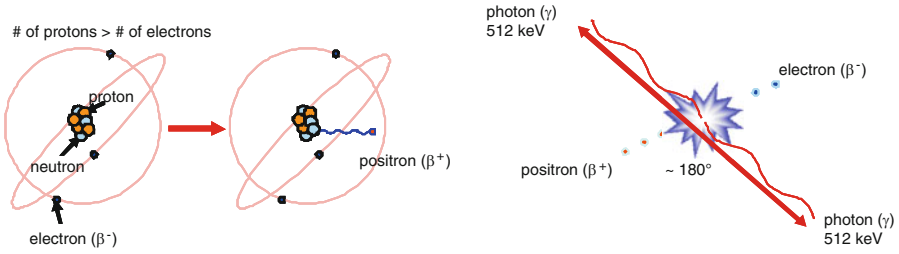

Fig. 2.2. *Positron generation and annihilation. Left*: positron emission from a radionuclide; *Right*: positron annihilation, which generates two annihilation photons or gamma photons

fed to a coincidence module, which examine whether two pulses are truly due to the annihilation process. The smaller the difference between the two pulses, the closer the detection stems from the true annihilation event. Modern electronics, however, can measure time with a resolution of 10^{-8} s or larger. As a result, the event is registered as coincidence only if a pair of detectors (opposite to each other) detects the signal simultaneously within a certain time window. The coincident time window used is in the range of 10 ns.

2.2.2 Image Reconstruction

In a typical PET scan, 10^6–10^9 events (decays) are detected depending on the radioactivity injected and the time of measurement. Coincidence events are saved as the special data set called sinogram. The sinogram is the line-integral projection data obtained from a large number of detectors at different views surrounding the entire object. The sinogram data is used to reconstruct an image through mathematical algorithms such as analytical or iterative reconstruction methods. Analytical methods calculate the radionuclide tracer distribution directly from the measured sinogram data. Backprojection and Filtering (BF) or Filtered Backprojection (FB) are typical algorithms used for analytical methods. They require less computational burden than statistical methods such as the Expectation Maximization (EM) algorithm. Analytic approaches, however, often suffer from an artifact known as the streak artifact, which arises from the physical gaps existing between the detectors. In contrast, iterative methods like EM reconstruct the image in an iterative fashion using the measured sinogram. Iterative methods, therefore, are often more robust to noise, such as streak artifacts, and can provide better Signal to Noise Ratio (SNR) at a given spatial image resolution. Although iterative methods require much more computational burden, due to the recent improvement of computing technologies and algorithms, EM algorithm is now widely used as the main stream method of PET image reconstruction.

2.2.3 Signal Optimization

In addition to the basic image reconstruction, it is important to note that there are several physical phenomena, such attenuation, scattering, and random coincidences, which are necessary to correct when more quantitatively accurate PET images are required. Interactions within the body with incident photons, which result in scattering and attenuation, are known as scatter and coincidence events, respectively, and require correction. The scattered coincidence events and attenuation corrections are two major problems together with accidentally-occurring coincidence events. In addition, the efficiency of each detector may vary between each detector and influence the measured data. Therefore, various correction techniques have been developed to correct the effect of attenuation, scatters, and random events. Only when these corrections schemes are completely incorporated into the main reconstruction algorithm,

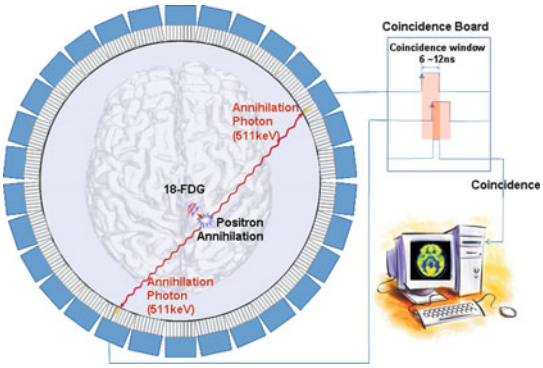

Fig. 2.3. *PET system components.* The simplified diagram shows the ring detector system and the coincident board, which is fundamental for image reconstruction in the computer

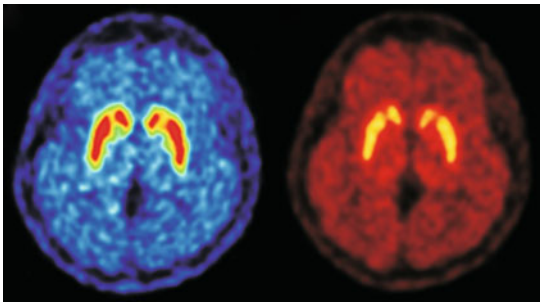

Fig. 2.4. *PET image examples.* The PET images of dopamine transporter and receptor binding using ^{18}F-FP-CIT and ^{11}C-Raclopride radionuclides are displayed as examples of how PET can be used for the measurements of neural status of the brain

PET can quantitatively image various radio-labeled ligands binding to specific receptors, transporters, and enzymes. This quantitatively calibrated molecular imaging is one of the strengths of PET imaging. For example, the interaction and distribution of the dopamine transporters or receptors in the brain can be measured using a PET with ^{18}FluoroPropyl-CarbomethoxyIodophenylnorTropane (F-FP-CIT) or ^{11}C-Raclopride (Figs. 2.3, 2.4).

2.2.4 High-Resolution Research Tomograph

One of the most advanced PET scanners is the High-Resolution Research Tomograph (HRRT), which has been introduced by Siemens. HRRT-PET is designed to obtain the highest spatial resolution and the highest sensitivity known in human brain PET imaging [6]. In contrast to the commercial PET, which usually has a system diameter of more than 80 cm to accommodate the whole body, the system diameter of HRRT-PET is only 46.7 cm, which is only suitable for a human brain scan. This small system diameter improved each detector's solid angle and, therefore, the sensitivity. In addition, the HRRT-PET has a longer axial Field-of-View (FOV) of 25.2 cm, as compared with the conventional PET, which has only 17 cm of axial FOV. The shorter system diameter and the longer axial FOV provide a dramatically improved detection efficiency, and thereby enhance the overall system sensitivity. With this increased sensitivity, HRRT-PET provides a considerably high

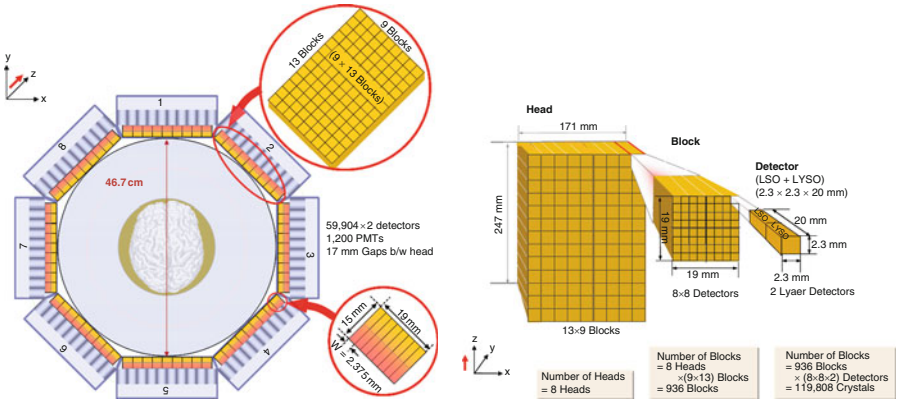

Fig. 2.5. *Detector configuration of HRRT-PET.* The HRRT-PET detector system consists of eight heads (*left*). Each head has 13 × 9 detector blocks build with two layers of 8 × 8 detectors. This results in a total of 119,808 scintillation detector crystals with dimension of 2.3 × 2.3 × 10 mm^3. These small detector crystals are packed in the form of a mosaic panel (*right*)

spatial resolution together with the small detector size, which has dimensions of 2.3 mm × 2.3 mm for width and height, respectively (Fig. 2.5).

This high spatial resolution combined with enhanced sensitivity [7, 8] makes the HRRT-PET the most advanced PET scanner for human brain studies [9]. Simultaneously, the improved spatial resolution reduces partial-volume effects, thereby improving quantification of metabolic rates in the brain such as the regional Cerebral Metabolic Rate of Glucose (rCMRGlc) [10]. In addition, transmission images are also obtained, supporting a more accurate attenuation and scatter correction.

These improvements in performance by the brain optimized configuration of the HRRT provided better imaging and allowed us to image smaller Region of Interest (ROI) than the previously available. In addition to PET's ability to measure and visualize metabolism, the distribution of neuroreceptors and neurotransporter in the brain can be measured. Also, HRRT-PET now allows the ability to measure the specific distribution of different ligands in various neurodegenerative disorders [10]. According to recent report, many small brain structures can be studied due to the availability of HRRT-PET [10,11]. These structures include:

1. The dopamine transporter-enriched nuclei in the midbrain where the dopaminergic cell bodies are located [12].
2. The substantia nigra, from which dopaminergic neurons projecting to the dorsal striatum.
3. The ventral tegmental area, from where neurons project to the limbic regions and the cerebral cortex [13].

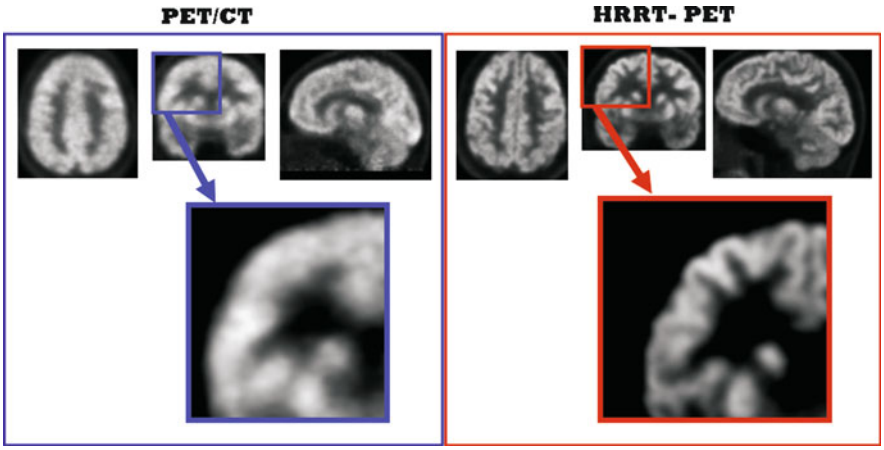

Fig. 2.6. *Resolution of HRRT-PET.* A section of the brain is captured with currently available PET scanner (*left*) and the HRRT-PET (*right*), which shows much more details and higher resolution

Other small regions such as the ventral striatum are actively pursued in search of potential ROIs for HRRT-PET research. Even arterial blood sampling in the human brain using the HRRT-PET is being studied by several groups [9,13].

The previously mentioned features made HRRT-PET have the one of the highest sensitivities and spatial resolutions among any currently available PET scanners. In Fig. 2.6, two comparative ^{18}F-Fludeoxygloucose (FDG) PET images emphasize the clear advantage of HRRT-PET over a conventional PET. In these images, the cortical gyri are seen much clearer with HRRT-PET than with PET/CT, suggesting that the HRRT can more accurately localize the molecular interactions in the brain than any other PET system available today.

2.3 Magnetic Resonance Imaging

2.3.1 Basic Principles

The main components of the MRI system are the main magnet, the Radio Frequency (RF) system, the gradient coil, the shim system, and the computer. The main magnet generates a strong magnetic field, which determines the imaging power of MRI. Permanent magnets and resistive magnets can be used to produce the external magnetic field; however, they are unable to produce high magnetic fields and are only used for the low field MRI. Today, the main magnetic field is commonly produced by a superconducting magnet maintained at a very low temperature. The superconducting electromagnet

consists of a coil that has been made super-conductive by a cooling system, which often consists of liquid helium surrounded by liquid nitrogen. By cooling, the superconductor becomes resistance free, which means large amounts of current can flow through the coil to produce high magnetic fields.

Once the coil becomes a superconducting magnet, it is capable of producing strong and stable magnetic fields suitable for MRI applications. The superconducting wire is usually made of Niobium-Titanium (NbTi), a rigid material that is simple to handle. Once a magnet is constructed with the strong magnetic field, one can insert an object which has spins of nuclei such as water protons. The spins in the object then will be aligned either parallel or anti-parallel to the main magnetic field. A slightly larger fraction of these protons will be oriented in the anti-parallel form and lead to a net magnetization. In a given magnetic field, all the spins precess with the specific frequency known as the Larmor frequency, which is specific to the strength of the magnetic field. If an external magnetic field or energy oscillating at the Larmor frequency is applied to the spins, the spins absorb the applied energy and are excited to the high energy status due to the magnetic resonance absorption phenomena.

The external energy is usually delivered by RF coils, which transmit RF energy to the object with a specific resonance frequency, often within a certain bandwidth that has a center frequency equivalent to the Larmor frequency. The precessing spins with the corresponding frequency at the non-excited or resting states are then flipped to a higher excited state where they last for a certain time depending on the relaxation properties of the object. The excited spins will return to the steady state and give off energy in the form of an electromagnetic signal or radiation, which is referred to as the Free Induction Decay (FID) signal. During the spin flips, the large numbers of small electrical dipoles, which are proportional to the resonant proton density, induce current on the RF coils that are surrounding the object. The simplest form of an RF system is composed of a transmitter coil and receiver coil. The RF system is an antenna which is sending excitatory RF pulses to the object or brain and also receiving the signals generated from the object. RF coils are one of the key components that determine the SNR of images. The development of specific purpose RF coils, therefore, is one of the central themes of MRI research.

2.3.2 Image Reconstruction

Each signal received by the antenna or RF coil contains information of the total sum of the object signals, but they are not encoded to produce an image yet. Formation of MRI requires the magnetic gradients to encode spatial information to the object. The gradient system has various functions such as slice selection, spatial encoding, spoiling, rewinding, echo production, and pre-saturation, among others. Among them, slice selection and spatial encoding are the most essential functions of the gradients system to spatially localize

the magnetic resonance signal. There are three gradient coils located within the bore of the magnet, which are wrapped along three orthogonal axes. The gradient is called according to the axis along which they act when switched on. For example, G_x is assigned for the horizontal axis of the magnet bore and alters the field along the x-axis.

These magnetic gradients are referred to as slice-selection gradient (G_z), phase-encoding gradient (G_y), and frequency-encoding frequency-encoding gradient or readout gradient (G_x), respectively. Slice selection gradients are usually applied at the RF excitation period so that only spins within a slice corresponding to the specific RF bandwidth are excited. Frequency-encoding or phase-encoding gradients are typically applied during or before data acquisition. This encoding scheme encodes spatial information into the RF signal. The received signal is in the spatial frequency domain, what is called k-space, equivalent to the 2D or 3D Fourier transform of the object.

2.3.3 Signal Optimization

The raw field produced by a superconducting magnet is approximately 1,000 parts per million (ppm) or worse, thus the magnetic field has to be corrected or shimmed. The shim system is used to correct field inhomogeneity and optimize for each imaging session. Field homogeneity is measured by examining an FID signal in the absence of field gradients. Shimming is important for a number of imaging applications. Most modern MRI techniques such as Echo Planar Imaging (EPI) and Chemical Shift Imaging (CSI) require homogeneous magnetic fields to be less than 3.5 ppm over the imaging volume. Usually this is accomplished by a combination of current loops (active or dynamic shim) and ferromagnetic material (passive or fixed shim). Gradient coils are used to provide a first-order shim. Since the introduction of a patient also distorts the magnetic field, often an active shim correction is made before scanning.

The signals that are detected via the RF coils are recorded in the computer system, and an image is reconstructed using a mathematical algorithm, such as the Fourier transform. The complexity of modern MRI arises mainly due to the many physical parameters involved such as spin relaxations of different kinds, for example spin-lattice and spin-spin relaxation times (T1 and T2), respectively. Most of the conventional imaging utilizes these magnetic properties, such as T1, T2, and susceptibility. In simple terms, the T1 value is the recovery time of the flipped spins and determines the interactions between spins and its surrounding lattice (tissue). The T2 value is the dephasing time of the in-phased spins due to spin-to-spin interaction, and the susceptibility is a spin dephasing factor due to surrounding magnetic fields. These magnetic properties can be weighted in the image by adjusting the pulse sequence and related imaging parameters.

In summary, MRI is a multi-purpose medical imaging instrument utilizing those intrinsic parameters mentioned and offers exquisite spatial resolution often more than an order of magnitude better than PET (Fig. 2.7). MRI,

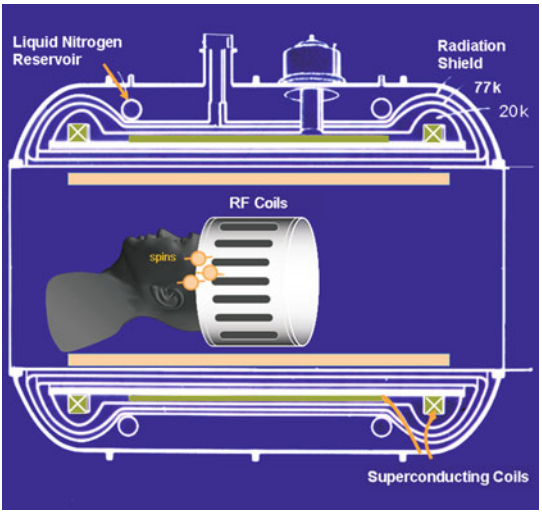

Fig. 2.7. *Diagram of MRI gantry.* The super-conduction coils are cooled with liquid nitrogen. The inner temperature is only 25 K

however, lacks molecular specificity, although a number of new techniques are being developed in combination with spectroscopic techniques or, more recently, with nano-particles.

2.3.4 High-Field MRI

The magnetic resonance signal is commonly proportional to the volume of data acquired and magnetic field strength. Therefore, high-field MRI systems provide an image with a higher SNR. In higher magnetic fields, it is possible to decrease the volume or voxel without sacrificing the SNR. It means that a high-field MRI system makes it possible to obtain higher spatial resolution and sensitivity than low-field MRI. Structural, metabolic, and functional assessments of an intact, living brain can be made using high-field MRI systems.

The 7.0 T MRI system, which uses an ultra-high field magnet, currently exists for human imaging with the high performance gradient coil set and RF coils. It provides us with many exquisite high-resolution images with an extremely high SNR. Recently, many ultra high-resolution images were obtained from 7.0 T MRI (Figs. 2.8, 2.9). Many fine structures, which were once thought impossible to image using MRI, were observed in the brain in vivo. The structures include the substantia nigra, red nucleus, and cerebral peduncle or crus cerebri in the midbrain. As demonstrated in Fig. 2.8a, the red nucleus and substantia nigra are clearly visible. In addition, the image of the cerebral peduncle surrounding the substantia nigra shows not only the fine vascular structures but also the fibers, suggesting that the details of ultra-fine high-resolution images can be of great help in identification of various neurological disorders and in the planning of surgical operations in a

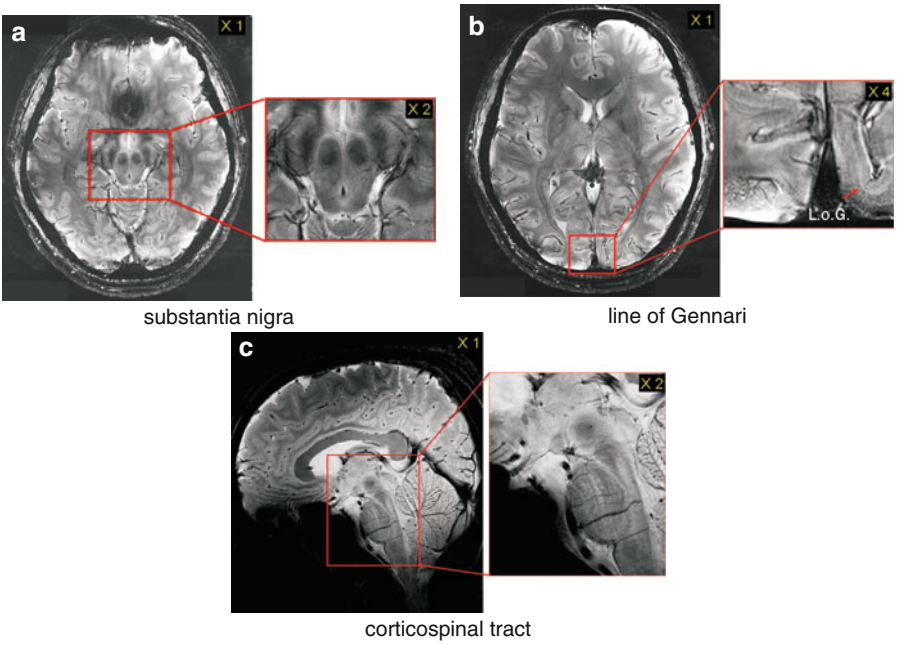

Fig. 2.8. *High-field MRI image examples.* The brain images are obtained from the 7.0 T MRI. In contrast to previous MRI systems, details of brain substructures can now be observed

totally non-invasive manner. The line of gennari in the visual cortex (Fig. 2.8b) and the perforating arteries and the corticospinal tracts in the pontine area (Fig. 2.8c) are also visualized in the 7.0 T MRI. Note the details of the thalamic area and the structures of the deep gray and white matter areas, like the anterior commissure, the mammillary body, and the red nucleus.

The substantia nigra is an important region in the area of Parkinson's disease research. Figure 2.9a and b are images of the central midbrain areas obtained from the same subject using 1.5 T and 7.0 T, respectively. As seen, 7.0 T MRI images are far superior and clearer than 1.5 T, particularly, in the boundary between the substantia nigra and surrounding tissues in 7.0 T MRI. Since the substantia nigra is believed to include iron, it is darker than other regions due to T2-related signal reduction. Likewise, the structure of the hippocampus and the parahippocampal regions, major ROI in the Alzheimer's studies, were clearly visualized by T2-weighted imaging in vivo by using 7.0 T MRI (not shown here). 7.0 T MRI began to show possible visualization of micro-vascular structures, such as the Lenticulostriate Arterie (LSA) in the human brain, which would be extremely useful for clinical purposes. Recently, we have reported regarding the advancements in micro-vascular imaging, such as the in vivo visualization of LSAs, which was once thought to be impossible [14].

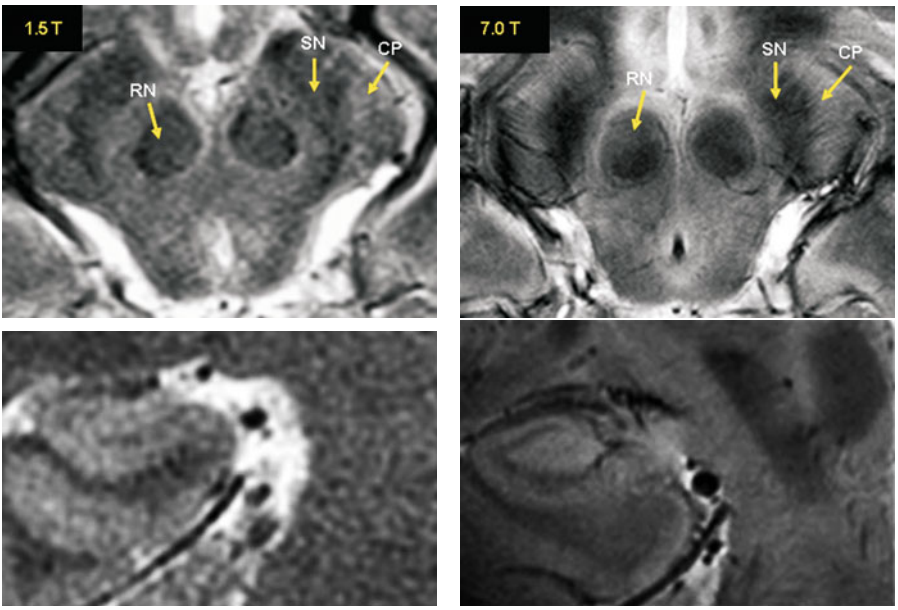

Fig. 2.9. *High- and low-field MRI.* Resolution in 1.5 T images (*left*) is lower as compared to 7.0 T (*right*), as it can be seen in the substantia nigra (*top*) and hippocampal region (*bottom*)

2.4 Hybrid PET Fusion System

PET is one of the most widely used imaging tools in both clinical areas as well as neuroscience research, especially for its ability to perform non-invasive, in vivo imaging of biochemical changes. PET can show how well tissues are working by the consumption of the amount of nutrients, neurotransmitter bindings, and blood flow within the tissue. In addition, there have been many new developments in radiopharmaceutical ligands and probes. PET uses various radioactive pharmaceuticals as tracers, which make it possible to detect molecular changes down to the pico-molar range. It has allowed us to look at in vivo physiology as well as the molecular chemistry of living humans non-invasively and has opened up modern quantitative molecular neuroscience. PET applications also expanded to the study of amino acid metabolism ([Methyl-^{11}C]-L-Methionine) and gene proliferation ^{18}F-L-Thymidine (FLT). PET has changed classical nuclear imaging concepts and has led to an entirely new domain of molecular imaging. Various radionuclide tracers of PET are listed in Table 2.2. Depending on the radionuclides and their labeled compounds, various PET imaging techniques are available [15–22].

Although PET provides direct information about tracer uptake into the cell for specific tissues, the spatial resolution of PET is poor in comparison to CT or MRI. As of today, 2.5 mm FWHM is the best spatial resolution that

Table 2.2. *Radionuclide tracers for PET [23].* The generation of the nuclides ^{11}C, ^{13}N, ^{15}O, ^{18}F, and ^{124}I requires a cyclotron

Hemodynamic parameters	H_2 ^{15}O, ^{15}O-butanol, ^{11}CO, $^{13}NH_3$
Hypoxia or angiogenesis	^{18}FMSIO, ^{64}Cu-ATSM, ^{18}F-Galacto-RGD
Substrate metabolism	^{18}F-FDG, $^{15}O_2$, ^{11}C-acetate
Protein synthesis	^{11}C-Methionine, ^{11}C-leucine, ^{11}C-tyrosine
DNA synthesis	^{18}F-FLT, ^{11}C-thymidine, ^{18}F-fluorouracil
Drugs	^{11}C-Cocaine, ^{13}N-cisplatin, ^{18}F-fluorouracil
Receptor affinity	^{18}F-FESP, ^{18}F-FP-Gluc-TOCA,^{18}F-FES
Gene expression	^{18}F-FHBG, ^{18}F-Penciclovir, ^{18}I-FIAU
Antibodies	^{124}I-CEA mimibody, ^{64}Cu-DOTA Her2/*neu* minibody

PET can have [24]. This resolution is still relatively poor for the localization of many delicate organs in the brain, such as the sub-regions in hippocampus.

In order to overcome its limitations, combining PET images with other high-resolution morphological imaging modalities such as radiography, CT and MRI has been studied [25–27]. Combining two or more imaging modalities is probably the best solution, especially in the field of neurological imaging.

In the past, to combine two different modalities, software registration has been used, and it works well in some studies where resolution requirement is relatively low.

2.4.1 PET/CT Systems

PET/CT is the first successful product in this series of research. Although it was the simple overlay of two images based on a mechanically calibrated shuttle bed or table, high-resolution anatomical images from CT partially aided the PET image, which has poor spatial resolution. The hybrid PET/CT imaging system can provide the functional image of PET with the superior anatomical delineation of CT. For example, PET/CT provides better distinction between cancerous tissue and healthy tissue in the diagnosis of cancer and the planning of radiation therapy.

2.4.2 PET/MRI Systems

On the other hand, magnetic resonance has much greater soft tissue contrast than CT, making it especially useful in neurological, musculoskeletal, cardiovascular, and oncological imaging. Unlike CT, it uses no ionizing radiation. Instead, it uses a powerful magnetic field to align the magnetization of hydrogen atoms in the body and provides excellent tissue contrasts in both brain and body imaging.

MRI has many advantages, such as its nonhazardous nature, high-resolution capability, potential for chemically specified imaging, capability of obtaining cross-sectional images in any desired directions, ability to use a

large variety of high tissue contrasts, diffusion imaging capabilities, flow-related imaging capabilities, and ability to perform functional MRI [28]. MRI is, therefore, preferred to CT in the new fusion imaging system.

In contrast to PET/CT, which provides the simple combination of functional and anatomical images, PET/MRI could provide the complex combination of various functional information, such as PET, functional MRI (fMRI) or Magnetic Resonance Spectroscopy (MRS), and detailed morphological information through using soft tissue contrasts, for example. Thus, the PET/MRI system allows us to complement quantitative biological functional information from PET, such as metabolisms and binding potentials, with the high-resolution morphological information or other functional information from MRI. When PET/MRI fusion images are available, perhaps unique biochemical and molecular information with high resolution will be obtained from our body, especially where high-resolution imaging is of utmost importance, such as the brain.

Fusion Concepts

A major obstacle in developing a fusion PET/MRI system is that conventional PET uses PMTs for detector components. Because PMTs are very vulnerable to magnetic fields, especially in ultra high-field MRI such as 7.0 T, the unacceptably large stray magnetic fields from MRI practically prohibit any close positioning of the PET to the MRI.

In order to alleviate this problem, two types of approaches have been suggested [29–40]:

1. Fiber optics is used to relay the scintillation light from detection crystals to the PET modules, which would be located outside the magnetic field of the MRI. Since the scintillation crystals and optic fibers are not sensitive to the magnetic field, this arrangement would be suited for the PET/MRI combination. Fiber optics, however, attenuate the optical signals and, therefore, degrade the overall sensitivity and spatial resolution.
2. APD and a semiconductor-type PMT in the PET/MRI fusion system is used. APDs can replace PMTs since they are insensitive to magnetic fields. Although APDs have been used successfully on small scale PET scanners for animal use, APD-based PET appears to suffer from long term stability.

Extensive research is still ongoing and some progress have been be achieved. In 2008, Judenhofer et al. developed an APD-based PET and MRI hybrid imaging system for animal use [41]. In three-dimensional (3D) animal PET, the APD-based and magnetically compatible scanner can be inserted into an animal 7.0 T MRI system to simultaneously acquire functional and morphological PET/MRI images from living mice. With this PET/MRI system, they have found a tumor hidden in tissue through using high-resolution magnetic resonance data and simultaneously determined whether it is malignant by functional PET data.

A PET/MRI hybrid system for humans using this APD-based PET insertion is being developed by Siemens, Inc. and the Max Plank Institute in Germany. This human PET/MRI consists of an APD based PET-insert and a low field MRI (3.0 T MRI) system. Other companies and institutions are also developing integrated PET/MRI systems using a 3 T or 1.5 T MRI [36–39]. The major obstacle of this integrated PET/MRI system appears to be the stability of APD circuitry due to interference with the magnetic fields and radiofrequency waves from the MRI unit. It has been reported that there is significant variation of the timing resolution of the APDs, thereby increasing the coincidence timing window up to 40 ns, compared to less than 10 ns in most of the current PET systems [36].

2.4.3 High-Resolution Fusion

In order to avoid these interferences and to fully utilize the molecular imaging capability of PET and the anatomical imaging capability of UHF-MRI such as 7.0 T in human imaging, each scanner can be operated separately and connected using a high precision mechanical shuttle bed. This configuration shares many characteristics with the current PET/CT configuration [42, 43]. In this manner, one can conveniently avoid any possible artifacts due to the magnetic field interference incurred with PET-inserts or magnetic field influencing the PET operation. The major drawback of this approach is that image acquisition is performed sequentially rather than simultaneously.

In 2007, Cho et al. [23] developed this kind of PET/MRI hybrid system using shuttle bed system. One of the major differences of the system with others is the coupling of two high-end systems, i.e., HRRT-PET and 7.0 T MRI, was achieved without any compromise. For molecular imaging, HRRT-PET is used and provides a spatial resolution of 2.5 mm FWHM, the highest resolution among the human PET systems, and 7.0 T MRI system for the highest resolution anatomical imaging. These two devices together will provide the highest sensitivity and resolution molecular information, further aided by sub-millimeter resolution 7.0 T MRI imaging.

The conceptual design of the new fusion PET/MRI is shown in Fig. 2.10. PET and MRI are installed as closely as possible. The two are connected by a shuttle system composed of a bed and its guided rails. Proper magnetic and RF shielding was designed both in the PET side as well as shuttle bed to avoid interference of strong magnetic fields of the 7.0 T MRI. The shuttle system is designed to fulfill the mechanical precision of less than 0.05 mm and is able to operate under a high magnetic field, such as 7.0 T. This precision is sufficient to meet the spatial resolution of the 7.0 T MRI so that HRRT-PET images are precisely guided into the desired neuroanatomical region(s). The major advantage of this type PET/MRI system is that it allows the exploitation of the best qualities of the two systems, i.e., the available resolution and sensitivity of HRRT-PET and UHF 7.0 T MRI without any compromise and interference.

Fig. 2.10. *PET/MRI fusion system.* The system combines by two separate high-end imaging devices (*top*), the HRRT-PET (*left*) and the 7.0 T MRI (*right*) by means of a high-precision shuttle railway system (*bottom*)

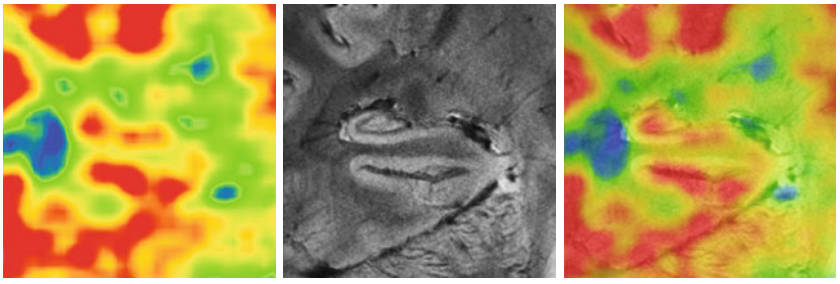

Fig. 2.11. *PET/MRI fusion image example.* The functional HRRT-PET image (*left*) and the high-resolution 7.0 T MRI image (*middle*) are overlaid (*right*) providing full diagnostic information

Critical issues for the success of this approach are the design and development of precision mechanics including the shuttle and railway, proper magnetic shield, and image fusion algorithm. The calibration method is also one of the important components of this system to correctly align the image coordinates of both imaging systems.

2.4.4 PET/MRI Fusion Algorithm

Two approaches are under development to integrate anatomical and molecular information. One is the image visualization approach and the other is the image restoration approach.

Image Visualization Approach

Most of the functional or molecular images, by themselves, cannot easily localize their signal origin. Overlaying the molecular information onto the structural image greatly improves the ability to characterize the desired anatomical location in the brain or organs [25–27, 44–46]. Advancement in image fusion methods allow for blending of higher spatial information of anatomical images with the higher spectral information of functional or molecular images (Fig. 2.11). These methods are classified into two categories by the fusion domain:

- Principal Component Analysis (PCA) [47], the Brovey method, and the Hue Intensity Saturation (HIS) method [48] are fused in the spatial domain.
- Discrete Wavelet Transform (DWT) and "A-trous" wavelet methods are fused in the transform domain [49, 50].

There are several ways to represent the color information depending on the color models: Red, Green, Blue (RGB), Cyan, Magenta, Yellow (CMY), and Intensity, Hue, Saturation (IHS). In some cases, the color transform between color models, such as RGB and IHS, is useful to combine the information from the multiple sensors.

$$C_{\mathrm{IHS}} = M \cdot C_{\mathrm{RGB}} \qquad \text{or} \qquad C_{\mathrm{RGB}} = M - 1 \cdot C_{\mathrm{IHS}} \tag{2.1}$$

where

$$C_{\mathrm{RGB}} = \begin{bmatrix} R \\ G \\ B \end{bmatrix}, \quad C_{\mathrm{IHS}} = \begin{bmatrix} I \\ v_1 \\ v_2 \end{bmatrix} \tag{2.2}$$

and

$$M = \begin{bmatrix} \frac{1}{3} & \frac{1}{3} & \frac{1}{3} \\ -\frac{\sqrt{2}}{6} & -\frac{\sqrt{2}}{6} & \frac{\sqrt{2}}{3} \\ \frac{1}{\sqrt{2}} & -\frac{1}{\sqrt{2}} & 0 \end{bmatrix}, \quad M^{-1} = \begin{bmatrix} 1 & -\frac{1}{\sqrt{2}} & \frac{1}{\sqrt{2}} \\ 1 & -\frac{1}{\sqrt{2}} & \frac{1}{\sqrt{2}} \\ 1 & \sqrt{2} & 0 \end{bmatrix} \tag{2.3}$$

Hue and saturation information is obtained from the intermediate variables v_1 and v_2 as following

$$H = \tan^{-1}\left(\frac{v_2}{v_1}\right) \quad \text{and} \quad S = \sqrt{v_1^2 + v_2^2} \tag{2.4}$$

The IHS model separates the image information I into the spatial information, such as intensity, and spectral information, such as hue H and saturation S.

The most common method of image fusion using HIS model is to substitute the whole or partial information of intensity channel from the lower resolution I_L to the higher resolution I_H.

Brovey's method simply modifies the brightness information by multiplying the intensity ratio of the higher resolution and the lower resolution.

$$C'_{\mathrm{RGB}} = \gamma \cdot C_{\mathrm{RGB}} \quad \text{where} \quad \gamma = \frac{I_H}{I_L} \tag{2.5}$$

The PCA technique transforms the inter-correlated variables to the uncorrelated variables.

$$C_{\mathrm{PCA}} = \Phi \cdot C_{\mathrm{RGB}} \quad \text{where} \quad C_{\mathrm{PCA}} = \begin{bmatrix} PC1 \\ PC2 \\ PC3 \end{bmatrix}, \quad \Phi = \begin{bmatrix} \varphi_{11} & \varphi_{12} & \varphi_{13} \\ \varphi_{21} & \varphi_{22} & \varphi_{23} \\ \varphi_{31} & \varphi_{32} & \varphi_{33} \end{bmatrix} \tag{2.6}$$

The hue and saturation is obtained in a similar way as the HIS method.

$$H = \tan -1 \left(\frac{PC3}{PC2} \right) \quad \text{and} \quad S = \sqrt{PC2^2 + PC3^2} \tag{2.7}$$

The primary component $PC1_H$ of the higher resolution image replaces the one $PC1_L$ of the lower resolution in the image fusion algorithm. The PCA fusion has the advantage of minimally distorting the spectral characteristics.

The wavelet transform method can be applied to the image fusion based on the multi-resolution analysis approach.

$$C_{\mathrm{RGB}} = R_{\mathrm{RGB}} + [W_{\mathrm{RGB}}]_n \tag{2.8}$$

where

$$R_{\mathrm{RGB}} = \begin{bmatrix} R_r \\ G_r \\ B_r \end{bmatrix}, \qquad [W_{\mathrm{RGB}}]_n = \begin{bmatrix} \sum_{k=1}^{n} W_{R,k} \\ \sum_{k=1}^{n} W_{G,k} \\ \sum_{k=1}^{n} W_{B,k} \end{bmatrix} \tag{2.9}$$

The C_{RGB} image is composed of a multi-resolution wavelet plane, $[W_{\mathrm{RGB}}]_n$, and the residual multi-spectral images, R_{RGB}. R_{RGB} and $[W_{\mathrm{RGB}}]_n$ contain the lower and higher spatial frequency of the image, respectively. For the image fusion, replacing wavelet coefficients $[W_{\mathrm{RGB}}]_{n,L}$ of the lower resolution image to the ones $[W_{\mathrm{RGB}}]_{n,H}$ of the higher resolution image.

Image Restoration Approach

Most of the functional or molecular images have lower resolution than anatomical images. For example, the intrinsic resolution of PET images is substantially poorer than MRI images. The intrinsic resolution of the PET system is determined mainly by the scintillation detector or crystal size and is approximately half of the detector width. The actual measured resolution is worse than the intrinsic resolution due to other image blurring factors, such as the

source size, the positron range, the traveling distance, the penetration effect due to the adjacent detectors, and the angular jitters due to variations in the angles of the annihilation photons. These blurring factors can be mathematically modeled as the spatially invariant system. Among the blurring factors, the source size and the positron range are source-dependent and spatially invariant factors, while the others are spatially variant.

For simplicity, PET system can be assumed to be the spatially invariant system and the system blurring can be defined as a Point Spread Function (PSF). Once the exact PSF of the system is properly estimated, it can be used for an image deblurring operation or deconvolution. The PET image deblurring operation can be performed using a number of parameters that are extractable from neurochemical and molecular information, as well as image resolution information obtainable from MRI. For example, it is well-known that glucose utilization within cells takes place in the gray matter rather than in the white matter or in the Cerebrospinal Fluid (CSF). To execute the PET/MRI image fusion process, an appropriate segmentation of MRI images is essential to separate the corresponding tissues (gray matter) from the others such as white matter and CSF [51]. From an actual image processing point of view, it is equivalent to deconvolution of the measured PET sinogram with a Gaussian PSF derived from the MRI data to enhance the resolution of the PET image [51–53]. It is often accomplished in an iterative fashion (Fig. 2.12). The resolution of molecular image of PET, which is usually much poorer than that of MRI, can be enhanced by combining the high-resolution image of MRI with additional information such as neurochemical or molecular a priori information, such as the potential neurophysiological location of

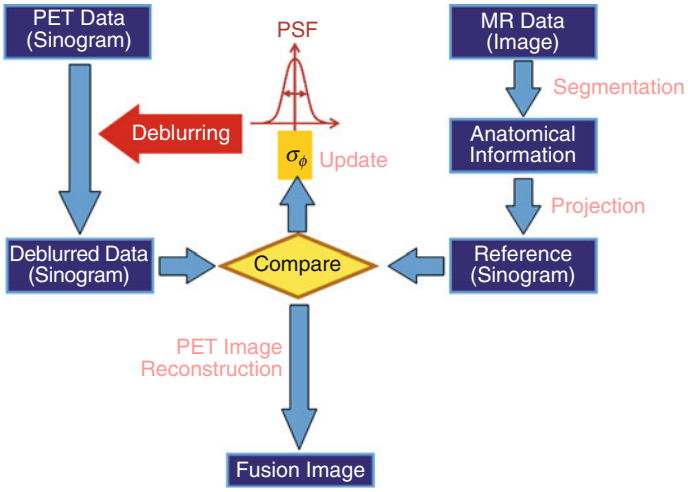

Fig. 2.12. *Iterative fusion algorithm.* The anatomical information of MRI data is utilized iteratively to confine the blurred PET image

receptor distribution for a particular ligand. In this fusion scheme, the segmented anatomical information from the MRI image is important and must be strongly correlated to the molecular information from the PET image.

Mismatched a priori information may cause over- or under-estimation of the PSF and the resultant fusion image may be biased. In order to utilize the anatomical image as a priori information, the contrast of the target tissue is also important. For instance, we know that the neuronal activities are generally confined to the gray matter rather than white matter, and segmentation of gray matter provides important morphological structures that can be registered with cortical activity (confined to the gray matter) as detected by FDG PET.

A preliminary human study was conducted to validate the usefulness of our fusion algorithm. A human brain image obtained by PET/MRI and the fusion algorithm is shown in Fig. 2.13, demonstrating that PET images can indeed be confined and localized with help of MRI, especially with an ultra high-resolution MRI such as the 7.0 T system.

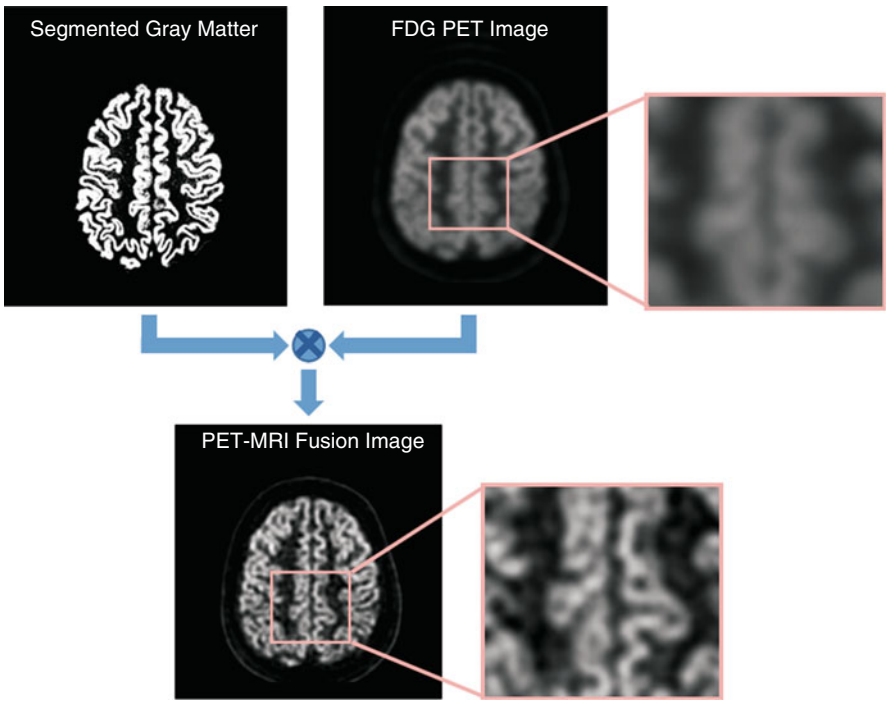

Fig. 2.13. *High-resolution PET/MRI fusion image of human brain.* The source images are obtained with the author's new PET/MRI fusion system. The spatial resolution of the PET is improved via the deblurring process based on the anatomical information of the MRI. The image data is processed in the sinogram domain

2.5 Conclusions

PET and MRI have been the most promising diagnostic tools among medical imaging tools, especially in the area of neuroscience. PET delivers information on molecular activities of human brain in vivo including enzymes and receptor distributions with resolutions down to 2.5 mm FWHM. On the other front, the MRI can obtain images with sub-millimeter resolution (down to 250 μm) and allows us to visualize the entire brain including the brain stem areas as well as other cortical and sub-cortical areas. For advanced and accurate diagnosis, these two systems are combined to overcome their limitations.

Although a few problems still remain, the current PET/MRI fusion system produces the highest quality images of molecular activities of the human brain in vivo and provides unprecedented molecular activity matched high-resolution images, which represent highly correlated molecular information to anatomically well established organs. This new PET/MRI fusion system, for the first time, began to provide anatomically well-defined molecular activities in the brain hitherto unavailable by any other imaging devices. This molecular fusion imaging system would be an important and essential tool for studying cognitive neurosciences and neurological diseases, such as the Parkinson's and Alzheimer's diseases. A mathematical image processing strategy that integrates anatomical and molecular information together is a still unfinished challenge in the field of medical image processing. We hope that the technology will provide novel and unique information to clinicians and research scientists in the field of neuroscience.

Acknowledgment

This work was supported by Basic Science Research Program through the National Research Foundation (NRF) funded by the Ministry of Education, Science and Technology (R11-2005-014 & 2008-04159).

References

1. Cho Z, Chan J. Circular ring transverse axial positron camera for 3-dimensional reconstruction of radionuclides distribution. IEEE Trans Nucl Sci. 1976;23(1):613–22.
2. Ter-Pogossian M, Phelps M. A positron-emission transaxial tomograph for nuclear imaging PET. Radiology. 1975;114(1):89–98.
3. Cho Z, Farukhi M. Bismuth germanate as a potential scintillation detector in positron cameras. Soc Nucl Med. 1977;18:840–44.
4. Melcher C, Schweitzer J. A promising new scintillator: cerium-doped lutetium oxyorthosilicate. Nucl Instrum Methods Phys Res. 1992;314:212–14.
5. Cho Z, Chan J. Positron ranges obtained from biomedically important positron-emitting radionuclides. Soc Nucl Med. 1975;16:1174–76.
6. Knoß C. Evaluation and Optimization of the High Resolution Research Tomograph HRRT. RWTH Aachen University, Aachen, Germany; 2004.

7. Eriksson L, Wienhard K, Eriksson M, et al. The ECAT HRRT: NEMA NEC evaluation of the HRRT system, the new high-resolution research tomograph. IEEE Trans Nucl Sci. 2002;49(5):2085–88.
8. De Jong H, Velden F. Performance evaluation of the ECAT HRRT: an LSO-LYSO double layer high resolution, high sensitivity scanner. Phys Med Biol. 2007;52(5):1505–26.
9. Mourik J, Velden F. Image derived input functions for dynamic high resolution research tomograph PET brain studies. Neuroimage. 2008;43(4):676–86.
10. Heiss W, Habedank B. Metabolic rates in small brain nuclei determined by high-resolution PET. J Nucl Med. 2004;45(11):1811–15.
11. Willeit M, Ginovart N. High-affinity states of human brain dopamine D2/3 receptors imaged by the agonist [11C]-(+)-PHNO. Biol Psychiatry. 2006;59(5):389–94.
12. Jucaite A, Fernell E. Reduced midbrain dopamine transporter binding in male adolescents with attention-deficit/hyperactivity disorder: association between striatal dopamine markers and motor hyperactivity. Biol Psychiatry. 2005;57(3):229–38.
13. Hirvonen J, Johansson J. Measurement of striatal and extrastriatal dopamine transporter binding with high-resolution PET and [(11)C]PE2I: quantitative modeling and test-retest reproducibility. J Cereb Blood Flow Metab. 2008;28(5):1059–69.
14. Cho Z, Kang C. Observation of the lenticulostriate arteries in the human brain in vivo using 7.0 T MR angiography. Stroke. 2008;39(5):1604–06.
15. Tjuvajev J, Stockhammer G. Imaging the expression of transfected genes in vivo. Cancer Res. 1995;55(24):6126–32.
16. Gambhir S, Barrio J. Imaging of adenoviral-directed herpes simplex virus type 1 thymidine kinase reporter gene expression in mice with radiolabeled ganciclovir. Soc Nuclear Med. 1998;39:2003–011.
17. Gambhir S, Bauer E. A mutant herpes simplex virus type 1 thymidine kinase reporter gene shows improved sensitivity for imaging reporter gene expression with positron emission tomography. Natl Acad Sci. 2000;97:2785–90.
18. Harrington K, Mohammadtaghi S. Effective targeting of solid tumors in patients with locally advanced cancers by radiolabeled pegylated liposomes. Proc Am Assoc Cancer Res. 2001;7:243–54.
19. Jacobs A, Braunlich I. Quantitative kinetics of [124I] FIAU in cat and man. J Nucl Med. 2001;42(3):467–75.
20. Jacobs A, Voges J. Positron-emission tomography of vector-mediated gene expression in gene therapy for gliomas. Lancet. 2001;358(9283):727–29.
21. Yaghoubi S, Barrio J. Human pharmacokinetic and dosimetry studies of [18F] FHBG: a reporter probe for imaging herpes simplex virus type-1 thymidine kinase reporter gene expression. Soc Nucl Med. 2001;42:1225–34.
22. Tjuvajev J, Doubrovin M. Comparison of radiolabeled nucleoside probes FIAU, FHBG, and FHPG for PET imaging of HSV1-tk gene expression. J Nucl Med. 2002;43(8):1072–83.
23. Cho Z, Son Y. A fusion PET-MRI system with a high-resolution research tomograph-PET and ultra-high field 7 T-MRI for the molecular-genetic imaging of the brain. Proteomics. 2008;8(6):1302–23.
24. Wienhard K, Schmand M. The ECAT HRRT: performance and first clinical application of the new high resolution research tomograph. IEEE Trans Nucl Sci. 2002;49(1):104–10.

25. Makela T, Pham Q. A 3-D model-based registration approach for the PET, MR and MCG cardiac data fusion. Med Image Anal. 2003;7(3):377–89.
26. Terence ZW, Timothy G. PET and brain tumor image fusion. Cancer J. 2004;10:234–42.
27. Borgwardt L, Hojgaard L. Increased fluorine-18 2-fluoro-2-deoxy-D-glucose FDG uptake in childhood CNS tumors is correlated with malignancy grade: a study with (FDG) positron emission tomography/magnetic resonance imaging coregistration and image fusion. J Clin Oncol. 2005;23(13):3030–37.
28. Cho Z, Jones J. Foundations of Medical Imaging. New York: Wiley-Interscience; 1993.
29. Garlick P, Marsden P. PET and NMR dual acquisition PANDA: applications to isolated, perfused rat hearts. NMR Biomed. 1997;10(3):138–42.
30. Shao Y, Cherry S. Simultaneous PET and MR imaging. Phys Med Biol. 1997;42(10):1965–70.
31. Shao Y, Cherry S. Development of a PET detector system compatible with MRI/NMR systems. IEEE Trans Nucl Sci. 1997;44(3):1167–71.
32. Farahani K, Slates R. Contemporaneous positron emission tomography and MR imaging at 1.5 T. J Magn Reson Imaging. 1999;9(3):497–500.
33. Slates R, Farahani K. A study of artefacts in simultaneous PET and MR imaging using a prototype MR compatible PET scanner. Phys Med Biol. 1999;44:2015–28.
34. Slates R, Cherry S. Design of a small animal MR compatible PET scanner. IEEE Trans Nucl Sci. 1999;46(3):565–70.
35. Marsden P, Strul D. Simultaneous PET and NMR. Br J Radiol. 2002;75:S53.
36. Catana C, Wu Y. Simultaneous acquisition of multislice PET and MR images: initial results with a MR-compatible PET scanner. J Nucl Med. 2006;47(12):1968–76.
37. Grazioso R, Zhang N. APD-based PET detector for simultaneous PET/MR imaging. Nucl Instrum Methods Phys Res. 2006;569(2):301–05.
38. Raylman R, Majewski S. Initial tests of a prototype MRI-compatible PET imager. Nucl Instrum Methods Phys Res. 2006;569(2):306–09.
39. Raylman R, Majewski S. Simultaneous MRI and PET imaging of a rat brain. Phys Med Biol. 2006;51(24):6371–80.
40. Raylman R, Majewski S. Simultaneous acquisition of magnetic resonance spectroscopy MRS data and positron emission tomography PET images with a prototype MR-compatible, small animal PET imager. J Magn Reson Imaging. 2007;186(2):305–10.
41. Judenhofer M, Wehrl H. Simultaneous PET-MRI: a new approach for functional and morphological imaging. Nat Med. 2008;14(4):459–65.
42. Kinahan P, Townsend D. Attenuation correction for a combined 3D PET/CT scanner. Med Phys. 1998;25(10):2046–53.
43. Beyer T, Townsend DW. A combined PET/CT scanner for clinical oncology. J Nucl Med. 2000;41(8):1369–79.
44. Barillot C, Lemoine D. Data fusion in medical imaging: merging multimodal and multipatient images, identification of structures and 3D display aspects. Eur J Radiol. 1993;17(1):22–27.
45. Rehm K, Strother SC. Display of merged multimodality brain images using interleaved pixels with independent color scales. J Nucl Med. 1994;35(11):1815–21.

46. Pietrzyk U, Herholz K. Clinical applications of registration and fusion of multimodality brain images from PET, SPECT, CT, and MRI. Eur J Radiol. 1996;21(3):174–82.
47. Gonzalez-Audicana M, Saleta J. Fusion of multispectral and panchromatic images using improved IHS and PCA mergers based on wavelet decomposition. IEEE Trans Geosci Remote Sens. 2004;42(6):1291–99.
48. Tu T, Su S. A new look at IHS-like image fusion methods. Info Fusion. 2001;2(3):177–86.
49. Wang A, Sun H. The application of wavelet transform to multi-modality medical image fusion. Proc IEEE ICNSC. 2006; p. 270–274.
50. Zheng Y, Essock E. A new metric based on extended spatial frequency and its application to DWT based fusion algorithms. Info Fusion. 2007;8(2):177–92.
51. Baete K, Nuyts J. Anatomical-based FDG-PET reconstruction for the detection of hypo-metabolic regions in epilepsy. IEEE Trans Med Imaging. 2004;23(4):510–19.
52. Gindi G, Lee M. Bayesian reconstruction of functional images using anatomical information as priors. Med Imaging. 1993;12(4):670–80.
53. Teo BK, Seo Y. Partial-volume correction in PET: validation of an iterative postreconstruction method with phantom and patient data. J Nucl Med. 2007;48(5):802–10.